Morphology analysis and process optimization of μ-SLA 3D manufactured micro-nano conic structure

Chongjun Wu
College of Mechanical Engineering, Donghua University, Shanghai, China
Yutian Chen
Saic Volkswagen Automobile Co. LTD, Shanghai, China
Xinyi Wei
College of Mechanical Engineering, Donghua University, Shanghai, China
Junhao Xu
Donghua University, Shanghai, China, and
Dongliu Li
Sicher Elevator Co., Ltd., Huzhou, China

Received 16 October 2023
Revised 6 December 2023
7 February 2024
Accepted 22 February 2024

Abstract

Purpose – This paper is devoted to prepare micro-cone structure with variable cross-section size by Stereo Lithography Appearance (SLA)-based 3D additive manufacturing technology. It is mainly focused on analyzing the forming mechanism of equipment and factors affecting the forming quality and accuracy, investigating the influence of forming process parameters on the printing quality and optimization of the printing quality. This study is expected to provide a μ-SLA surface preparation technology and process parameters selection with low cost, high precision and short preparation period for microstructure forming.

Design/methodology/approach – The μ-SLA process is optimized based on the variable cross-section micro-cone structure printing. Multi-index analysis method was used to analyze the influence of process parameters. The process parameter influencing order is determined and validated with flawless micro array structure.

Findings – After the optimization analysis of the top diameter size, the bottom diameter size and the overall height, the influence order of the printing process parameters on the quality of the micro-cone forming is: exposure time (B), print layer thickness (A) and number of vibrations (C). The optimal scheme is A1B3C1, that is, the layer thickness of 5 μm, the exposure time of 3000 ms and the vibration of 64x. At this time, the cone structure with the bottom diameter of 50 μm and the cone angle of 5° could obtain a better surface structure.

Authors' contributions: Chongjun Wu designed the whole conception and theoretical analysis. Yutian Chen, Xinyi Wei and Junhao Xu conducted the experiments and paper writing. Dongliu Li provided guides in the work implementation.

Funding: This work is supported in by the Fundamental Research Funds for the Central Universities (2232023D-15), the Shanghai Natural Science Foundation (22ZR1402400) and the China Postdoctoral Science Foundation (2022M721910). The authors wish to record the gratitude for the generous supports.

Competing interests: The authors declare that they have no known competing financial interests or personal relationships that could have appeared to influence the work reported in this paper.

Ethics approval: We confirm that this manuscript is original and has not been published, it is also currently not under consideration for publication elsewhere.

Journal of Intelligent Manufacturing and Special Equipment
Emerald Publishing Limited
e-ISSN: 2633-660X
p-ISSN: 2633-6596
DOI 10.1108/JIMSE-10-2023-0009

Originality/value – This study is expected to provide a μ-SLA surface preparation technology and process parameters selection with low cost, high precision and short preparation period for microstructure forming.

Keywords Micro-cone, Micro-nano additive manufacturing, Orthogonal experimental design, Process parameters optimization

Paper type Research paper

1. Introduction

The Stereo Lithography Appearance (SLA) is one of the most mature and high quality additive manufacturing technologies, which has obvious advantages of the rapid, cost-effective and high precision complex structure formation compared with the traditional machining methods (Li *et al.*, 2023a; Dong *et al.*, 2023; Shu *et al.*, 2022). The SLA method generally takes liquid photosensitive resin as molding material, adopts photoinitiated liquid material polymerization crosslinking curing and forms the final solid parts after layer by layer curing. Its potential industrial applications have been reckoned as cutting-edge technology in the next few years (Wu *et al.*, 2022a, b; Wang and Huang, 2022).

In recent years, SLA-based additive manufacturing technology has been widely developed, especially in biomedical research, industrial manufacturing and other fields due to its advantages of high precision and low cost in forming complex 3D structures in a relatively simple way (Jin *et al.*, 2021; Weng *et al.*, 2023; Liu *et al.*, 2021; Qu *et al.*, 2022). For example, the typical application can be found in the surface preparation for hydrophobic surfaces, which is generally difficult for the preparation technology with the traditional materials reduction method. Common methods for preparing superhydrophobic surfaces include laser processing (Liu *et al.*, 2023a; Zhan *et al.*, 2021), chemical etching technique (Kumar and Gogoi, 2018; Kim *et al.*, 2018), template method (Jiang *et al.*, 2016; Christian *et al.*, 2009), coating method (Shen *et al.*, 2021; Zhang *et al.*, 2021a), etc. However, these processing methods have typical features of high processing cost and complex process; the fabricated microstructures cannot be precisely controlled.

In order to understand the typical advantages of 3D SLA method in micro-nano manufacturing, researchers have carried out a lot of investigations on the molding process. Zhang *et al.*, (2021b) studied the shrinkage deformation of parts caused by material solidification in digital light processing molding technology (DLP) through the finite element simulation analysis and obtained the forming process parameters to reduce the shrinkage deformation. Guo *et al.*, (2022) introduced the microscopic dynamic mechanism of free base photopolymerization into the thick-time equation, revealing the change rule of curing thickness in DLP with initiator concentration and light intensity. Behera *et al.*, (2021) elaborated the forming constraints and solutions in the light curing micro-nano structure additive from the aspects of forming materials, machine resolution, part geometry and volume, etc. The results show that the expansibility of micro-scale additive manufacturing is improved. Li *et al.*, (2019) theoretically analyzed the relationship between the print thickness of photocuring and the exposure time, and the study showed that the step effect on the surface of parts could be significantly reduced by adopting the print layer thickness of 10 μm.

The SLA experimental equipment is similar to the current laser scanning, DLP and LCD photocuring 3D printing technology in forming mechanism (Korkunova *et al.*, 2022). The surface exposure molding method adopted by the optical path system of the liquid photosensitive equipment is different from the point exposure molding of traditional SLA, and is also different from the expensive digital projection light source of DLP and the low precision of LCD molding (Ozkan *et al.*, 2022). At present, the fabrication of microstructures by photocuring additive technology is still in the very early process, the influence of process parameters, molding accuracy and printing time on photocuring molding need to be further explored (Yusoff *et al.*, 2022; Yanar *et al.*, 2020). Meanwhile, it has important significance and potential application in academic research and improving economic benefits of enterprises (Farrell *et al.*, 2021; Sochol *et al.*, 2018).

Researchers (Rohita *et al.*, 2022) are constantly trying to print higher quality parts by optimizing printing process, materials, printing methods, etc. Since the cross-sectional area of the 2D parts manufactured by layers is always changing, and the surface of the 3D parts eventually formed will inevitably produce a stepped shape (Hu *et al.*, 2019). Therefore, it is particularly important to optimize the stepped effect of inclined plane structure parts as much as possible for the forming of micro-scale structure. Li *et al.*, (2023b) studied the relationship between selective laser sintering printing and parts structure performance by establishing neural network genetic algorithm and finally, increase the structural stiffness of printed parts by about 20%. Rendas *et al.*, (2023) studied the mechanical properties of 3D printing process parameters on tensile resistance and bending resistance of regular section parts structures by using range method and found that a thin printing layer thickness is conducive to improving the mechanical strength of the structure. Kafshgar *et al.* (Kafshgar *et al.*, (2021) analyzed the influence of 3D printing process parameters such as printing layer thickness and filling density on structural mechanical properties by using the variance analysis method and multi-objective optimization. At present, the research on process optimization mainly focuses on the modeling analysis and optimizing the forming process of 2D section parts such as rectangle. However, in the application of additive manufacturing, it is necessary to carry out further research on the forming of changing 2D section structure and the additive forming of variable cross-section micro-scale structure.

Therefore, this paper is devoted to prepare micro-cone structure with variable cross-section size by SLA-based 3D additive manufacturing technology. It is mainly focused on analyzing the forming mechanism of equipment and factors affecting the forming quality and accuracy, investigating the influence of forming process parameters on the printing quality and optimization of the printing quality. This study is expected to provide a μ-SLA surface preparation technology and process parameters selection with low cost, high precision and short preparation period for microstructure forming.

2. Experiments and process design

2.1 Experimental setup

The experiment is carried out on the micro-nano forming equipment developed by Shanghai Prismlab Electromechanical Technology Co., LTD in Figure 1. As can be seen, the equipment is mainly composed of three parts: computer, control system and printing device parts. The operating software of the computer in the equipment is used for model import, printing parameter setting and human–computer interaction. The control system is for receiving instructions from the computer to control the movement of the printing equipment. At the same time, it receives feedback information from the sensor in the printing device and feeds back the printing situation in real time. The printing device is responsible for receiving the instructions sent by the computer and the control system and printing the task.

The technical parameters of the experimental equipment include the printing length, width and height of the photocuring molding range in 36.48*20.52*30 mm. The printing accuracy is 3.2 μm, the resolution is 1.6 μm, while the thickness of the printing layer is between 5 and 40 μm. According to the requirements of equipment adaptation and molding accuracy in this experiment, the photosensitive resin material used in this experiment is composed of C, O and N elements with C content of 78.23%, O content of 18.54% and N content of 3.22% in Figure 2.

Among the main parameters of the resin, the hardness after curing is 80–90 HD, the bending strength is 90–112 MPa and the tensile strength is 35–42 MPa (Chen *et al.*, 2023). Since the post curing process will affect the mechanical properties, thus the properties show a variational range. In this paper, the curing time is keeping constant at 10 min.

2.2 Defects in molding

Quality defect is the most difficult problem in parts forming, which will seriously affect the forming quality and production efficiency of parts. The forming defects are mainly related to the forming

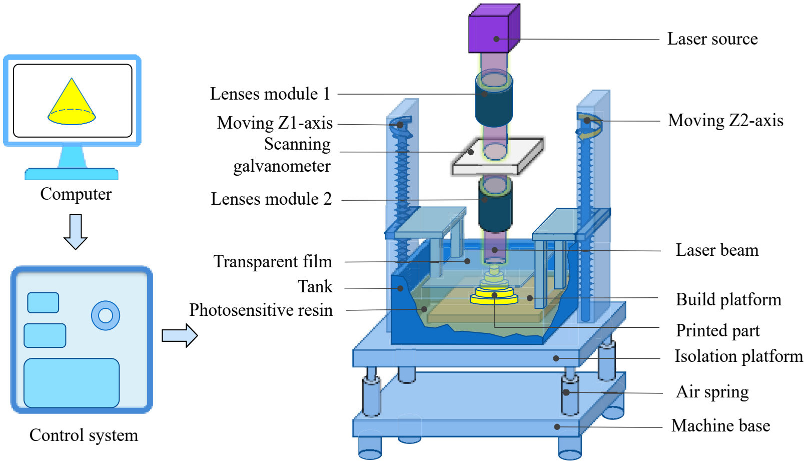

Source(s): Authors' own creation/work

Figure 1.
3D printing equipment setup

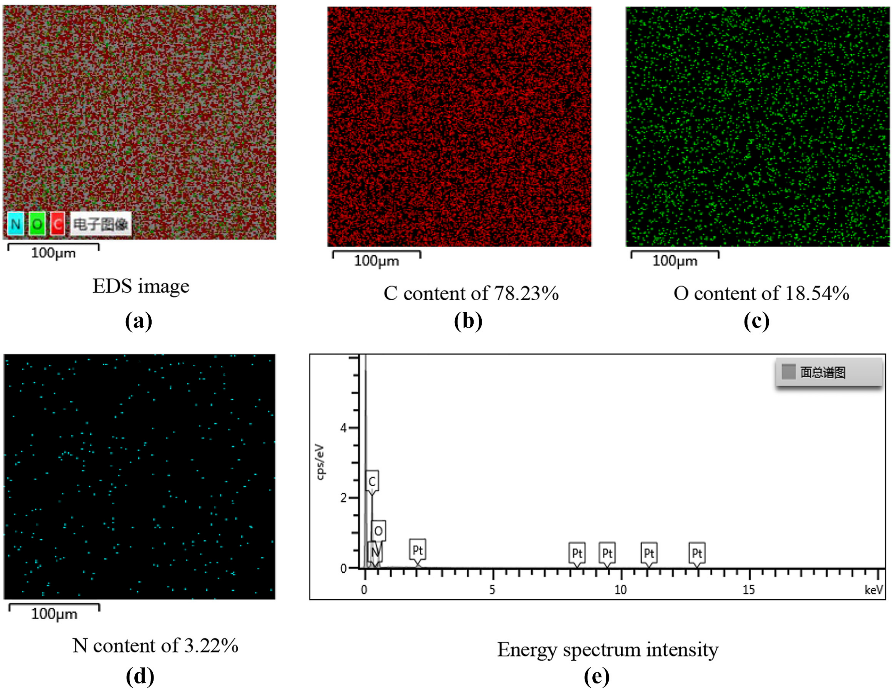

Source(s): Authors' own creation/work

Figure 2.
EDS for element distribution of the photosensitive resin

accuracy, model structure, printing process parameters and post-processing technology of the equipment, among which the printing process parameters have the most obvious influencing effect on the forming quality of the parts. Printing process parameters mainly include printing layer thickness, exposure time and vibration frequency. The thickness of the printing layer determines the printing molding time. The smaller the thickness, the smoother the surface of the parts, while this will take a longer printing time; On the contrary, the thicker the printing layer, the more difficult it is for light energy to pass through the resin, thus a rough surface with bad quality. The exposure time will affect the x, *y* and *z* axis of the printed structure. If the exposure time is too long, the liquid photosensitive resin will absorb more light energy and fully cured, so that the actual print size is larger than the designed size. The number of vibrations mainly affects the zoom ratio of light spot. The larger the number of vibrations, the larger the reduction ratio of light spot.

The defect morphology under environmental scanning electron microscope (ESEM) in this test is shown in Figure 3 Figure 3(a) reflects the quality defect of the cone molding, which is generally absent from the print molding of the tiny cone angle at the top. Figure 3(b) reflects that although the conic structure is printed as a whole, there is a quality problem that half of the tip cone corner is formed and half is missing. Figure 3(c) reflects the mass defects of the cone with a diameter of 50 μm at the bottom, with obvious stratification, stepped structure, curved top and missing cone top.

2.3 Orthogonal experiment design

Orthogonal test method is a scientific and reasonable arrangement of tests for multiple factors and multiple levels of change (Liu *et al.*, 2023b; Chen *et al.*, 2022). In the orthogonal test, the results of the experimental study are called evaluation indexes, the influencing factors related to the experimental evaluation indexes are called factors and the variation of factors is called levels. As shown in Figure 4, if all the trial groups are tested, at least 256 trials are required to be conducted. Massive repetitions of the test are unfavorable to the analysis of the test results. If the orthogonal test is adopted, the test results can be analyzed by adopting only 16 tests.

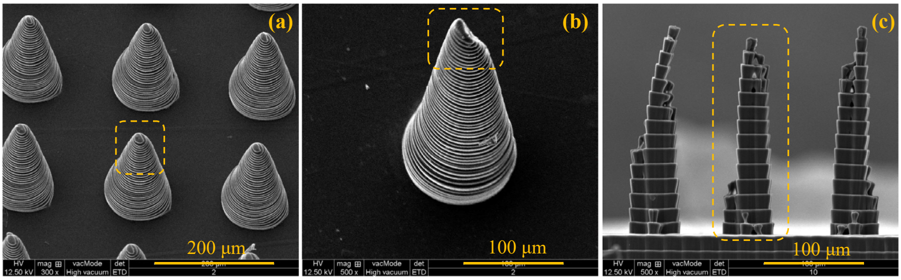

Note(s): (a) Conic array; (b) Enlarged zone of (a); (c) Front view of the flawed cone structure
Source(s): Authors' own creation/work

Figure 3. SEM image for typical defect characteristics

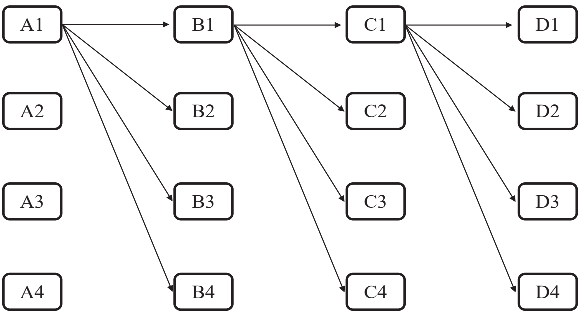

Source(s): Authors' own creation/work

Figure 4. Comprehensive test of the orthogonal method

When the orthogonal test table is designed, each factor is arranged in a row, and the change of each factor is symmetrical horizontally. In this way, the parameters of each group in the orthogonal test group will contain one of the variation levels of all the factor objects studied in the orthogonal test. All levels of change for each factor occur equally in all orthogonal trials.

In this paper, there are three factors in the orthogonal test, namely, print layer thickness (A), exposure time (B) and vibration frequency (C). The orthogonal test of three factors and three levels was carried out. The values of test factors and levels were shown in Table 1.

The orthogonal test group is planned as shown in Table 2, which is divided into nine groups, and each factor formed a column in the table. The change level of each factor was equal for three times, and the parameters in the different nine groups of orthogonal experiment were printed for three parts under the same parameters.

The selection of printing parameters is mainly related to the three-dimensional structure size of the model. Before choosing these parameters, preliminary preparation tests were conducted to set the reasonable process parameters zone. Finally, the printing thickening selection is 5–15 μm, the exposure time is 2000–3,000 ms, the vibration frequency is 64–144x. For example, if the thickness of the printing layer is less than 5 μm, due to the mechanical accuracy of the machine Z axis, it is difficult to ensure the molding quality. In the meanwhile, when the layer thickness is greater than 20 μm, the slicing layer thickness is too large and the printed pyramidal structure ladder morphology is very apparent, and the top structure is easy to bend or miss when forming. When the exposure time is lower than 2000 ms, the top structure of the cone is often difficult to form; when the exposure time is greater than 3,000 ms, the diameter of the cone will be thickened; the number of vibrations mainly determines the number of scanning during the light curing time.

2.4 Test model design

Different from the cylinder structure from the bottom to the top printing constant cross-section, the cone structure in the printing process of printing the size of the section is getting smaller, small size means more prone to printing bending, breaking, mucosa and other problems, so the

Table 1.
Factor level table

Levels	Factors Print layer thickness(A)/μm	Exposure time (B)/ms	Number of vibrations(C)/x
1	5	2000	64
2	10	2,500	100
3	15	3,000	144

Source(s): Authors' own creation/work

Table 2.
Orthogonal test table

Tests No	Print layer thickness(A)/μm	Exposure time(B)/ms	Number of vibrations(C)/x
1	5	2,000	64
2	5	2,500	100
3	5	3,000	144
4	10	2,000	100
5	10	2,500	144
6	10	3,000	64
7	15	2,000	144
8	15	2,500	64
9	15	3,000	100

Source(s): Authors' own creation/work

precision of molding equipment and process parameters higher requirements. As shown in Figure 5, the cone structure of the variable section model has a diameter of 50 μm at the bottom and 1 μm at the top, the angle is 5°, the center spacing is 100 μm, and arranged in a row. The cone structure is a process of variable cross-section molding, and the size of the cone top is close to 1 μm, which is far lower than the conventional light curing 3D printing 50 μm molding level, undoubtedly more stringent requirements for printing equipment and process parameters. This will also help to achieve a better printing quality in complex structures printing.

3. Morphology analysis for conical structure

Additive manufacturing process is to process 3D printing data into 2D data through slicing software, and then print 3D solid parts by stacking and accumulating layers. Therefore, the surface of parts formed by additive manufacturing will leave layered morphology of additive forming. When the structure with irregular curved surface such as inclined plane or circular arc is manufactured by additive manufacturing, this layered step morphology is more obvious due to the additive mechanism, as shown in Figure 6. For the microstructure additive forming, the surface topography of the parts will seriously affect the surface quality of the parts and even lead to the parts difficult to form. Therefore, the main analysis of this experiment by controlling the thickness of the printing layer, exposure time and vibration times, so as to reduce the shape of the step, and print out the tiny structure.

Surface morphology could well reflect the manufactured quality, which could help to understand the process effect on the structure (Zhou *et al.*, 2021; Li *et al.*, 2023c). Environmental scanning electron microscope (QUANTA 250, Czech Republic) was used to observe the array cone at different magnifications of 500, 1,000 and 2,500 X. Fig.s 7, 8 and 9 show the three-dimensional ESEM morphology with nine sets of parameters and different printing parameters, the test numbers correspond to serial numbers (a), (b) and (c) in the figure, respectively.

According to the 500X magnification of nine groups of parameters in Figures 7, 8 and 9, the 3D morphology of the cone basically conforms to that of the originally designed cone structure, but there is a big difference in morphology. In the microscopic morphology at

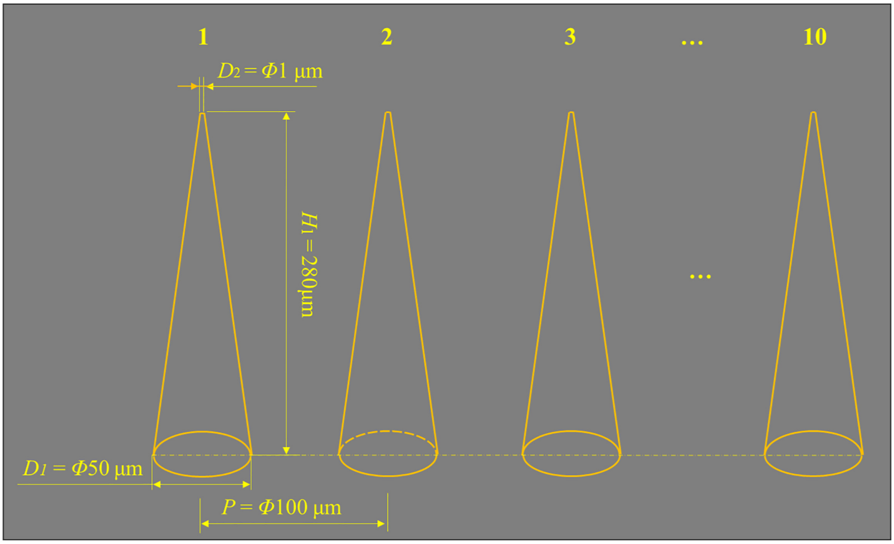

Source(s): Authors' own creation/work

Figure 5.
3D model structure and size of the cone

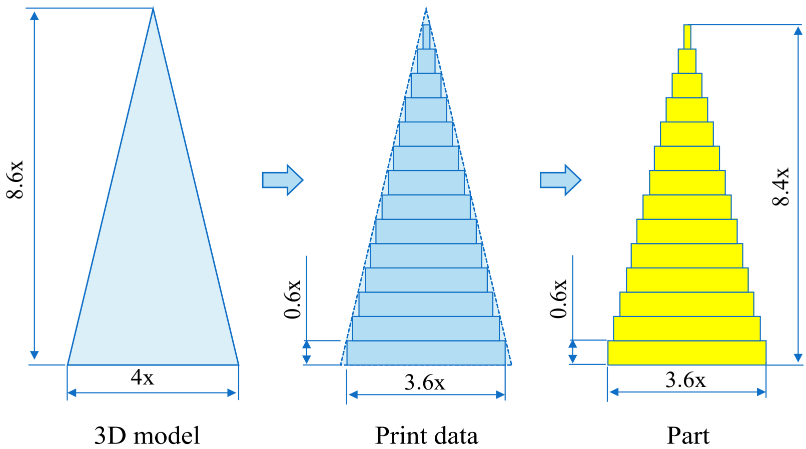

Figure 6.
3D data and actual molded parts

Source(s): Authors' own creation/work

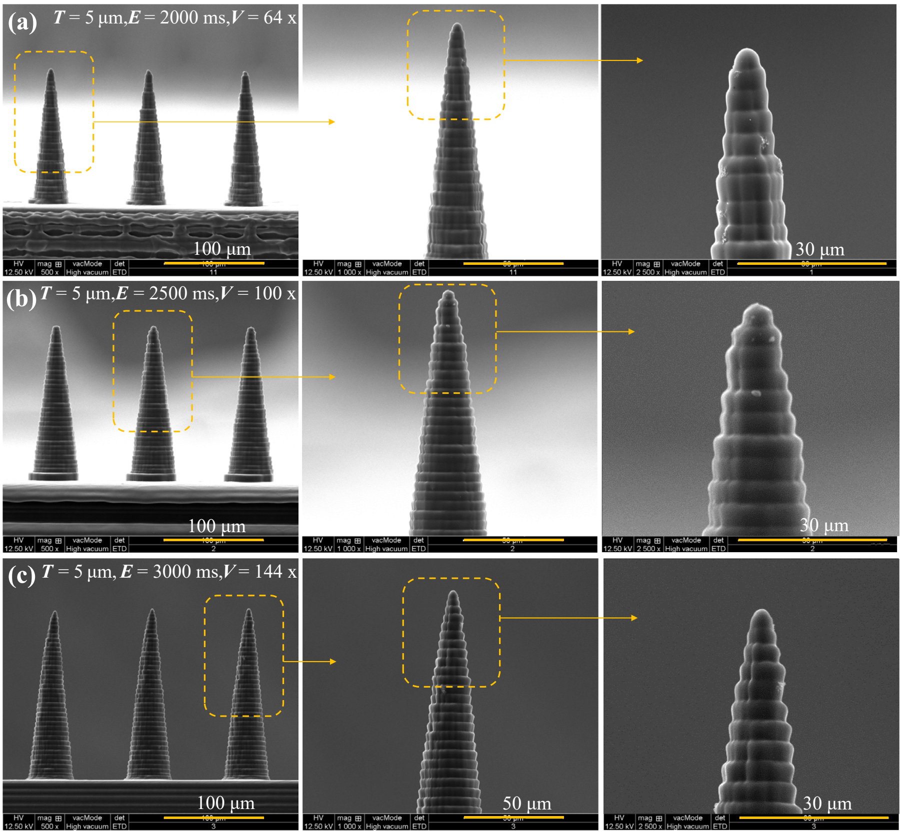

Figure 7.
3D SEM morphology for Test No. 1, 2 and 3 at print layer thickness of 5 µm

Source(s): Authors' own creation/work

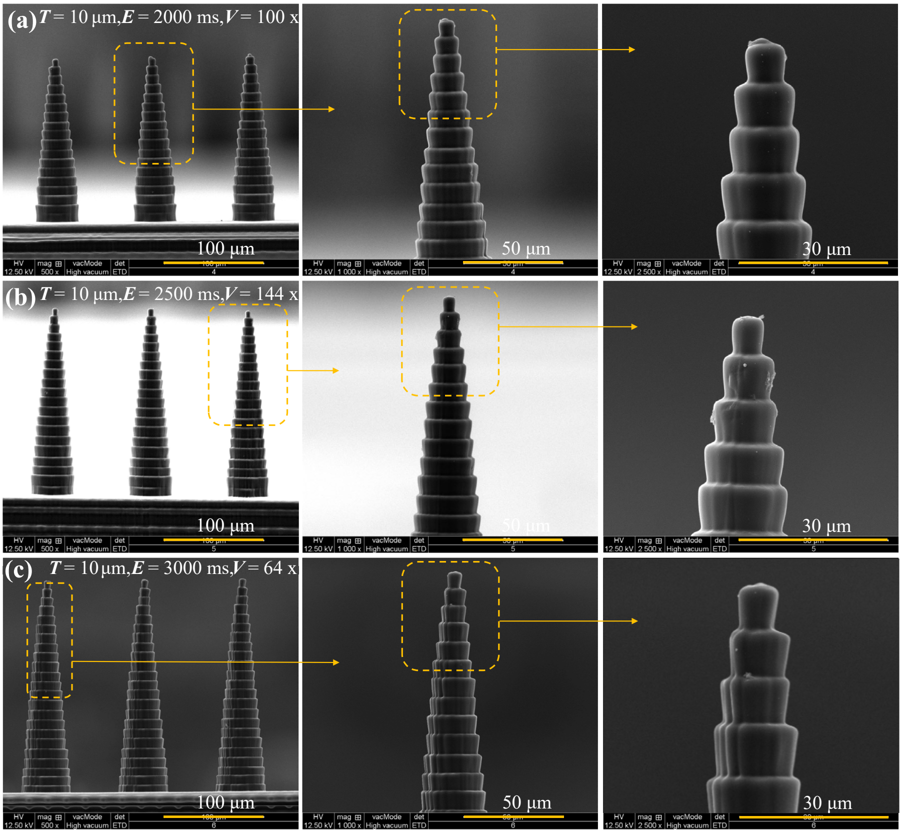

Source(s): Authors' own creation/work

Figure 8.
3D SEM morphology for Test No. 4, 5 and 6 at print layer thickness of 10 μm

1,000X magnification, the thickness of (a), (b) and (c) in Figure 7 is 5 μm, that of (a), (b) and (c) in Figure 7 is 10 μm and that of (a), (b) and (c) in Figure 8 is 15 μm. The height and overall shape of the cone are different. At 1,000X magnification, the layering phenomenon of the cone with variable cross-section from the bottom to the top becomes more apparent due to the different thickness of the printing layer. At 2,500X magnification, the cone surface roughness and the diameter of the apex are also different.

The conical surface is close to the smooth transition in Figure 7, circular cone top part also is similar to the smooth transition arc shape and accordingly from cone top diameter is relatively small. Compared to 10 μm thickness layer of Figures 8 and 15 μm thickness layer of Figure 9, 5 μm thickness layer of the surface of Figure 7 shows a more drastic surface roughness change. In Figure 8, with the change of section size, the conical surface has similar stepped morphology between layers. The morphology of the conical surface tends to be simple stepped morphology. In Figure 9, the morphologies of the cone are different between layers, and the changes of the steps between layers are more obvious, and the position of the cone top is similar to the shape of an inverted round table.

4. Optimization of result analysis

The printing of conical structure is different from the uniform section of cylinder. It is a variable section printing and forming way, which increases the overall difficulty in printing and printing

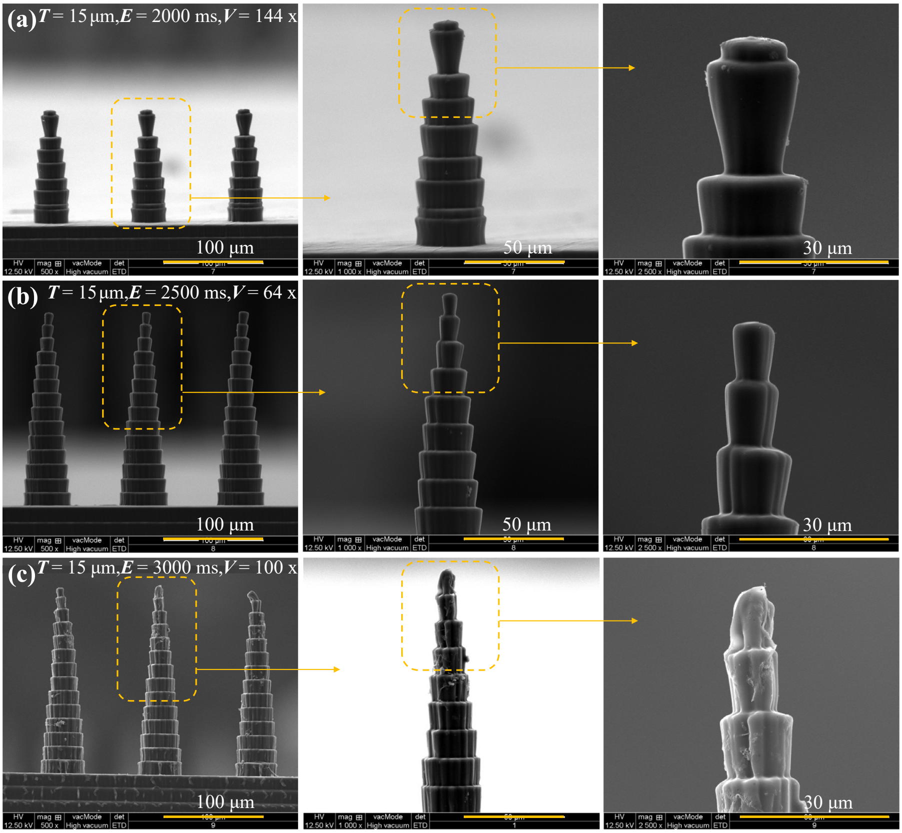

Source(s): Authors' own creation/work

Figure 9.
3D SEM morphology for Test No. 7, 8 and 9 at print layer thickness of 15 µm

parameters, will definitely affect the quality of printing. The printing error of micro-cone includes the top diameter error, the bottom diameter error, the overall height error and the relationship between the top diameter errors, the bottom diameter error and printing parameters is obvious. Therefore, the multi-index analysis method is used to analyze the test data.

The measurement of the cone size is shown in Figure 10. During the measurement, the top diameter, the bottom diameter and overall height of the micro-cone structure are measured, and the three cones are measured, respectively. Finally, the average value of the measurement results is taken.

After calculating the average value, the top diameter, the bottom diameter and overall height of the cone can be used to measure the size error of the cone structure, and the calculation equation is shown in equation (1).

$$\Delta D_2 = |D_0 - D_1| \tag{1}$$

In the equation, ΔD_2 is the absolute error, µm; D_0 is the design size value, µm; D_1 is the average value of actual size measurement, µm.

4.1 Single index analysis

During the measurement, the top diameter, the bottom diameter and the overall height were measured according to the ratio of magnification of the scanning electron microscope images. The

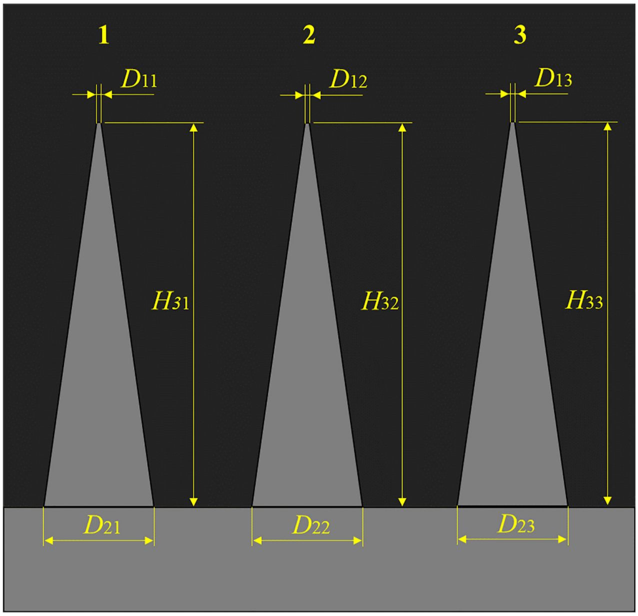

Source(s): Authors' own creation/work

Figure 10. Measurement positions and corresponding size

measurement results were averaged and the absolute error value was used to measure the size error of the cone structure. The absolute error of the top diameter is Δd, the absolute error of the bottom diameter is ΔD and the absolute error of overall height is ΔH. The error results of measuring cone structure under nine groups of different process parameters are shown in Table 3.

The results of the orthogonal test were processed by the range analysis method, which can analyze the influence of each factor on printing quality, optimal level and optimal parameter combination of each group of measurement results of orthogonal test. The range analysis of size error is shown in Tables 4–6.

For the optimization analysis of the top diameter index of the printed cone, in the three groups of tests with the same layer thickness level of factor A, the range R is 5.036, which indicating that there is a difference of 5.036 in the influence of the layer thickness on the top diameter. The range of exposure time B is 2.382 and the range of vibration number 0.533. It

Tests no	Print layer thickness(A)/μm	Exposure time(B)/ms	Number of vibrations(C)/x	Δd	ΔD	ΔH
1	5	2,000	64	1.822	9.995	142.721
2	5	2,500	100	4.485	0.144	123.262
3	5	3,000	144	1.085	1.904	107.387
4	10	2,000	100	5.731	7.336	112.897
5	10	2,500	144	3.616	8.149	90.531
6	10	3,000	64	4.658	0.737	65.573
7	15	2,000	144	10.346	14.087	165.856
8	15	2,500	64	7.145	2.197	84.353
9	15	3,000	100	5.010	5.478	84.783

Source(s): Authors' own creation/work

Table 3. Orthogonal test table and test results

can be seen that the printing layer thickness has the highest influence on the printing quality, followed by the exposure time and finally, the number of vibrations. The best printing process is A1B3C1, that is, layer thickness 5 μm, exposure time 3,000 ms and vibration 64 x.

For the optimization analysis of the printed cone bottom diameter index, the range R is 3.240 in factor A, which means the difference of the influence of layer thickness on the bottom diameter index is 3.240. In this way, the range of exposure time B is 7.776, and the range of vibration number is 3.737. It can be seen that the exposure time has the greatest influence on print quality, followed by the number of vibration and the thickness of print layer has the least influence. The best printing process is A1B3C1, that is, layer thickness 5 μm, exposure time 3,000 ms and vibration 64 x.

The overall height of the printed cone was optimized by the index analysis. In the three groups of experiments with the same layer thickness level of factor A, the range $R = 34.790$, which means that the layer thickness of 10 μm and 5 μm has A 34.790 difference on the overall height of the printed cone. In this way, the range of exposure time B is 54.577 and the range of vibration number is 23.709. It can be seen that the exposure time has the highest influence on the print quality, followed by the

Table 4.
Range analysis table of top diameter index

	Print layer thickness(A)/μm	Exposure time(B)/ms	Number of vibrations(C)/x
K1	2.464	5.966	4.542
K2	4.668	5.082	5.075
K3	7.500	3.584	5.016
Range R	5.036	2.382	0.533
Optimal levels	A1	B3	C1
Primary and secondary factors	A	B	C
The optimal combination		A1B3C1	

Source(s): Authors' own creation/work

Table 5.
Range analysis table of the bottom diameter index

	Print layer thickness(A)/μm	Exposure time(B)/ms	Number of vibrations(C)/x
K1	4.014	10.473	4.310
K2	5.407	3.497	4.319
K3	7.254	2.706	8.047
Range R	3.240	7.776	3.737
Optimal levels	A1	B3	C1
Primary and secondary factors	B	C	A
The optimal combination		A1B3C1	

Source(s): Authors' own creation/work

Table 6.
Range analysis table of overall height index

	Print layer thickness(A)/μm	Exposure time(B)/ms	Number of vibrations(C)/x
K1	124.457	140.491	97.549
K2	89.667	99.382	106.981
K3	111.664	85.914	121.258
Range R	34.790	54.577	23.709
Optimal levels	A2	B3	C1
Primary and secondary factors	B	A	C
The optimal combination		A2B3C1	

Source(s): Authors' own creation/work

print layer thickness and the number of vibration has the least influence. The best printing process is A2B3C1, that is, layer thickness 10 μm, exposure time 3,000 ms and vibration 64 x.

4.2 Multi-index optimization analysis

The analysis of a single index can only reflect the effect of each factor on a single evaluation index, and the order of priority and the combination of optimal schemes are only for the evaluation of a single index. Because it cannot meet the scenario where multiple evaluation indexes meet simultaneously, comprehensive optimization analysis of multiple indexes is needed (Guo *et al.*, 2021).

The optimization analysis of multiple indexes needs to integrate the evaluation results of single indexes according to the comprehensive evaluation matrix. The specific matrix is shown in equation (2). Suppose n factors are considered in orthogonal experiment, and each factor has m change levels. If the expected index value is larger, makes $K_{ij} = k_{ij}$; otherwise, makes $K_{ij} = 1/k_{ij}$.

$$M = \begin{bmatrix} K_{11} & 0 & \cdots & 0 \\ K_{12} & 0 & \cdots & 0 \\ \cdots & \cdots & \cdots & \cdots \\ K_{1m} & 0 & \cdots & 0 \\ 0 & K_{21} & \cdots & 0 \\ 0 & K_{22} & \cdots & 0 \\ \cdots & \cdots & \cdots & \cdots \\ 0 & K_{2m} & \cdots & 0 \\ 0 & 0 & \cdots & 0 \\ 0 & 0 & \cdots & K_{n1} \\ 0 & 0 & \cdots & K_{n2} \\ \cdots & \cdots & \cdots & \cdots \\ 0 & 0 & \cdots & K_{nm} \end{bmatrix} \tag{2}$$

Factor layer matrix is shown in Equation (3), $T_i = 1/\sum_{j=1}^{m} K_{ij}$.

$$T = \begin{bmatrix} T_1 & 0 & 0 & 0 \\ 0 & T_2 & 0 & 0 \\ \cdots & \cdots & \cdots & \cdots \\ 0 & 0 & 0 & T_n \end{bmatrix} \tag{3}$$

The horizontal matrix is shown in Equation (4), and the range of test factors is s_i, makes $S_i = s_i / \sum_{i=1}^{n} s_i$.

$$S = \begin{bmatrix} S_1 \\ S_2 \\ \cdots \\ S_n \end{bmatrix} \tag{4}$$

The weight of a single index in the test among multiple indexes is shown in equation (5).

$$\omega = MTS \tag{5}$$

The comprehensive weight of the three indicators is shown in equation (6).

$$\overline{\varpi} = \frac{\omega_1 + \omega_2 + \omega_3}{3} \tag{6}$$

After the analysis of multiple indicators, the weight of multiple indicator parameters is calculated. The larger the weight value is, the closer the correlation is to the overall index of the test results. The index weight results are shown in Table 7, among which the comprehensive weight value of A1, B3 and C1 is the largest among all factor groups.

The molding analysis of conical structure includes the analysis of many index factors. After the optimization analysis of the top diameter size, the bottom diameter size and overall height of the printed cone, the order of the influence of printing process parameters on the forming quality of the micro-cone is as follows: exposure time (B), print layer thickness (A) and number of vibrations (C). A1B3C1, the layer thickness of 5 μm, exposure time of 3,000 ms and vibration of 64 x, is the optimal scheme for analyzing the results by calculating the weight of multiple indexes. After weight calculation and parameter analysis, the technological parameters can be considered reasonable.

5. Optimized SEM structures

The optimized test parameters were adopted to print the cone structure model, as shown in Figure 11. From the experiments, the cone diameter at the top was 2.876 μm, the cone diameter at the bottom was 49.519 μm and the overall height was 180.435 μm. Compared with the print quality without optimization, it shows that the experimental optimal scheme is consistent with the actual print optimization effect. In order to show the exact printing effect of the adopted process parameters, a set of micro-conic arrays are printed

Tests No	Weight categories	Top diameter weight ω_1	Bottom diameter weight ω_3	Overall height weight ω_2	The comprehensive weights $\overline{\varpi}$	Optimal solution
1	A1	0.341	0.088	0.096	0.1748	A1
2	A2	0.179	0.120	0.071	0.124	
3	A3	0.112	0.099	0.053	0.088	
4	B1	0.078	0.117	0.067	0.087	
5	B2	0.092	0.168	0.201	0.153	
6	B3	0.130	0.201	0.260	0.197	B3
7	C1	0.024	0.075	0.099	0.067	C1
8	C2	0.021	0.068	0.099	0.063	
9	C3	0.022	0.060	0.053	0.045	

Source(s): Authors' own creation/work

Table 7.
Analysis of multiple indicators

as shown in Figure 12. In this figure, it can be found that the printed surface shows great surface quality and consistency in array structures. This could help to improve the application of μ-SLA technology in more microstructure preparation.

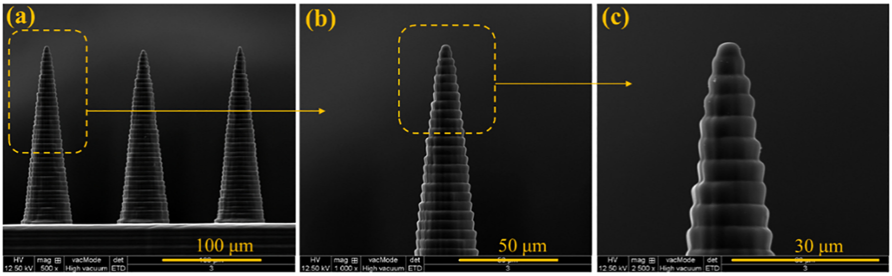

Source(s): Authors' own creation/work

Figure 11. Optimized cone structure under different magnification

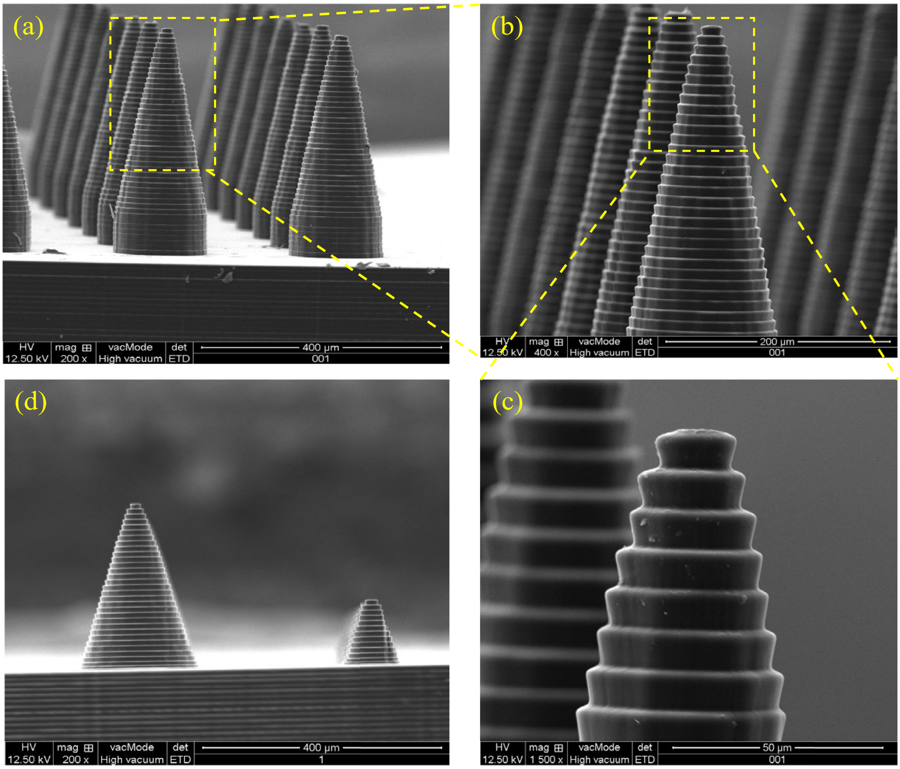

Note(s): (a) is the same size array, and (b) and (c) is the enlarged SEM zone; (d) is the micro array for different conic size

Source(s): Authors' own creation/work

Figure 12. The printed micro-conic array structure

6. Conclusions

In this paper, the μ-SLA additive manufacturing process parameters is optimized based on the variable cross-section micro-cone structure printing through detailed orthogonal experimental design. The multi-index analysis method was used to analyze the influence of process parameters through the forming quality of the top, bottom and overall height of the micro-cone. Furthermore, the process parameter influencing order is determined and validated with a series of experiments and final flawless micro array structure printing.

After the optimization analysis of the top diameter size, the bottom diameter size and the overall height, the influence order of the printing process parameters on the quality of the micro-cone forming is: exposure time (B), print layer thickness (A) and number of vibrations (C). The optimal scheme is A1B3C1, that is, the layer thickness of 5 μm, the exposure time of 3000 ms and the vibration of 64x. At this time, the cone structure with the bottom diameter of 50 μm and the cone angle of 5° could obtain a better surface structure. After the process optimization, the cone tip diameter could print to minimum diameter of 2.876 μm. Finally, all the optimized result is further validated through the flawless array structure printing.

References

Behera, D., Chizari, S., Shaw, L.A., Porter, M., Hensleigh, R., Xu, Z., Roy, N.K., Connolly, L.G., Zheng, X.R., Saha, S., Hopkins, J.B. and Cullinan, M.A. (2021), "Current challenges and potential directions towards precision microscale additive manufacturing-Part II: laser-based curing, heating, and trapping processes", *Precision Engineering*, Vol. 68, pp. 301-318, doi: 10.1016/j.precisioneng.2020.12.012.

Chen, S.S., Yang, S.M., Fai, C., Ho, L.T. and Zhang, F. (2022), "Suppression strategy of micro-waviness error in ultra-precision parallel grinding", *Nanomanufacturing and Metrology*, Vol. 5 No. 4, pp. 423-429, doi: 10.1007/s41871-022-00130-0.

Chen, Y.T., Wu, C.J., Wei, X.Y., Meng, X.K., Liu, J. and Wang, Q.B. (2023), "Morphology analysis and process optimization of micro-cylinder structure in micro-nano additive manufacturing", *Journal of Mechanical Engineering*, Vol. 59 No. 1, pp. 286-297.

Christian, W.J., Škereň, B.M., Najdek, D. and Černý, F. (2009), "Superhydrophobic surface structures in thermoplastic polymers by interference lithography and thermal imprinting", *Applied Surface Science*, Vol. 255 No. 23, pp. 9305-9310, doi: 10.1016/j.apsusc.2009.07.001.

Dong, Z., Yan, Y., Peng, G. and Geng, Y. (2023), "Effects of sandwiched film thickness and cutting tool water contact angle on the processing outcomes in nanoskiving of nanowires", *Materials and Design*, Vol. 225, 111438, doi: 10.1016/j.matdes.2022.111438.

Farrell, F.S., Ganonyan, N., Cooperstein, I., Moshkovitz, M.Y., Amouyal, Y., Avnir, D. and Magdassi, S. (2021), "3D-printing of ceramic aerogels by spatial photopolymerization", *Applied Materials Today*, Vol. 24, 101083, doi: 10.1016/j.apmt.2021.101083.

Guo, W., Wu, C., Ding, Z. and Zhou, Q. (2021), "Prediction of surface roughness based on a hybrid feature selection method and long short-term memory network in grinding", *The International Journal of Advanced Manufacturing Technology*, Vol. 112 No. 9, pp. 2853-2871, doi: 10.1007/s00170-020-06523-z.

Guo, T., Xia, M., Yang, W., Na, Q., Zhang, J., Yao, W., Yang, F. and Luo, Y. (2022), "Model of UV-curing thickness for new thiol-ene resin for additive manufacturing of energetic materials", *Additive Manufacturing*, Vol. 54, 102716, doi: 10.1016/j.addma.2022.102716.

Hu, G., Cao, Z., Hopkins, M., Hayes, C., Daly, M., Zhou, H. and Devine, D.M. (2019), "Optimizing the hardness of SLA printed objects by using the neural network and genetic algorithm", *Procedia Manufacturing*, Vol. 38, pp. 117-124, doi: 10.1016/j.promfg.2020.01.016.

Jiang, D., Fan, P., Gong, D., Long, J., Zhang, H. and Zhong, M. (2016), "High-temperature imprinting and superhydrophobicity of micro-nano surface structures on metals using molds fabricated by ultrafast laser ablation", *Journal of Materials Processing Technology*, Vol. 236, pp. 56-63, doi: 10.1016/j.jmatprotec.2016.05.009.

Jin, J., Mao, H. and Chen, Y. (2021), "Photocuring-while-writing: a 3D printing strategy to build free space structure and freeform surface texture", *Manufacturing Letters*, Vol. 29, pp. 113-116, doi: 10.1016/j.mfglet.2021.07.016.

Kafshgar, A.R., Rostami, S., Aliha, M. and Berto, F. (2021), "Optimization of properties for 3D printed PLA material using Taguchi, ANOVA and multi-objective methodologies", *Procedia Structural Integrity*, Vol. 34, pp. 71-77, doi: 10.1016/j.prostr.2021.12.011.

Kim, J.H., Mirzaei, A., Kim, H.W. and Kim, S.S. (2018), "Facile fabrication of superhydrophobic surfaces from austenitic stainless steel (AISI 304) by chemical etching", *Applied Surface Science*, Vol. 439, pp. 598-604, doi: 10.1016/j.apsusc.2017.12.211.

Korkunova, O.S., Kholkhoev, B.C. and Burdukovskii, V.F. (2022), "Photosensitive thiol–ene composition for DLP 3D printing of thermally stable polymer materials", *Mendeleev Communications*, Vol. 32 No. 2, pp. 231-233, doi: 10.1016/j.mencom.2022.03.026.

Kumar, A. and Gogoi, B. (2018), "Development of durable self-cleaning superhydrophobic coatings for aluminium surfaces via chemical etching method", *Tribology International*, Vol. 122, pp. 114-118, doi: 10.1016/j.triboint.2018.02.032.

Li, Y., Mao, Q., Li, X., Yin, J., Wang, Y., Fu, J. and Huang, Y. (2019), "High-fidelity and high-efficiency additive manufacturing using tunable pre-curing digital light processing", *Additive Manufacturing*, Vol. 30, 100889, doi: 10.1016/j.addma.2019.100889.

Li, C., Piao, Y., Zhang, F., Zhang, Y., Hu, Y. and Wang, Y. (2023a), "Understand anisotropy dependence of damage evolution and material removal during nanoscratch of MgF2 single crystals", *International Journal of Extreme Manufacturing*, Vol. 5 No. 1, 015101, doi: 10.1088/2631-7990/ac9eed.

Li, S., Wei, H., Yuan, S., Zhu, J., Li, J. and Zhang, W. (2023b), "Collaborative optimization design of process parameter and structural topology for laser additive manufacturing", *Chinese Journal of Aeronautics*, Vol. 36 No. 1, pp. 456-467, doi: 10.1016/j.cja.2021.12.010.

Li, C., Hu, Y., Zhang, F., Geng, Y. and Meng, B. (2023c), "Molecular dynamics simulation of laser assisted grinding of GaN crystals", *International Journal of Mechanical Sciences*, Vol. 239, 107856, doi: 10.1016/j.ijmecsci.2022.107856.

Liu, N., Ye, X., Yao, B., Zhao, M., Wu, P., Liu, G., Zhuang, D., Jiang, H., Chen, X., He, Y., Huang, S. and Zhu, P. (2021), "Advances in 3D bioprinting technology for cardiac tissue engineering and regeneration", *Bioactive Materials*, Vol. 6 No. 5, pp. 1388-1401, doi: 10.1016/j.bioactmat.2020.10.021.

Liu, S., Xiao, G., Lin, O., He, Y. and Song, S. (2023a), "A new one-step approach for the fabrication of microgrooves on Inconel 718 surface with microporous structure and nanoparticles having ultrahigh adhesion and anisotropic wettability: laser belt processing", *Applied Surface Science*, Vol. 607, pp. 15510801-15510818, doi: 10.1016/j.apsusc.2022.155108.

Liu, H., Fu, J., He, M., Hua, L. and Zhu, D. (2023b), "GWM-view: gradient-weighted multi-view calibration method for machining robot positioning", *Robotics and Computer-Integrated Manufacturing*, Vol. 83, 102560, doi: 10.1016/j.rcim.2023.102560.

Ozkan, B., Sameni, F., Bianchi, F., Zarezadeh, H., Karmel, S., Engstrøm, D.S. and Sabet, E. (2022), "3D printing ceramic cores for investment casting of turbine blades, using LCD screen printers: the mixture design and characterization", *Journal of the European Ceramic Society*, Vol. 42 No. 2, pp. 658-671, doi: 10.1016/j.jeurceramsoc.2021.10.043.

Qu, S.S., Yao, P., Gong, Y.D., Chu, D., Yang, Y., Wang, Z., Zhang, X. and Hou, Y. (2022), "Environmentally friendly grinding of C/SiCs using carbon nanofluid minimum quantity lubrication technology", *Journal of Cleaner Production*, Vol. 366, 132898, doi: 10.1016/j.jclepro.2022.132898.

Rendas, P., Figueiredo, L., Geraldo, M., Vidal, C. and Soares, B. (2023), "Improvement of tensile and flexural properties of 3D printed PEEK through the increase of interfacial adhesion", *Journal of Manufacturing Processes*, Vol. 93 No. 5, pp. 260-274, doi: 10.1016/j.jmapro.2023.03.024.

Rohita, P., Sohailb, B., Ashishc, S., Choubey, A. and Singh, S. (2022), "A process optimization of additive layer manufacturing processes for the production of polymer composite-based components", *Materials Today: Proceedings*, Vol. 60, pp. 1565-1569, doi: 10.1016/j.matpr.2021.12.083.

Shen, Y., Cai, Z., Tao, J., Li, K., Chen, H., Wu, Z. and Jia, Z. (2021), "Multi-type nanoparticles in superhydrophobic PU-based coatings towards self-cleaning, self-healing and mechanochemical durability", *Progress in Organic Coatings*, Vol. 159, 106451, doi: 10.1016/j.porgcoat.2021.106451.

Shu, C., Su, Q., Li, M., Wang, Z., Yin, S. and Huang, S. (2022), "Fabrication of extreme wettability surface for controllable droplet manipulation over a wide temperature range", *International Journal of Extreme Manufacturing*, Vol. 4, 045103, doi: 10.1088/2631-7990/ac94bb.

Sochol, R.D., Sweet, E., Glick, C.C., Wu, S.Y., Yang, C., Restaino, M. and Lin, L. (2018), "3D printed microfluidics and microelectronics", *Microelectronic Engineering*, Vol. 189, pp. 52-68, doi: 10.1016/j.mee.2017.12.010.

Wang, J. and Huang, G. (2022), "Review on manufacturing diamond abrasive tools by additive manufacturing technology", *Diamond andAbrasives Engineering*, Vol. 42 No. 3, pp. 307-316.

Weng, J., Saelzer, J., Berger, S., Zhuang, K., Bagherzadeh, A., Budak, E. and Biermann, D. (2023), "Analytical and experimental investigations of rake face temperature considering temperature-dependent thermal properties", *Journal of Materials Processing Technology*, Vol. 314, 117905, doi: 10.1016/j.jmatprotec.2023.117905.

Wu, C.J., Wei, X.Y., Chen, J., Liu, J., Guo, C., Wang, Q. and Liang, S.Y. (2022a), "Surface wettability analysis and preparation of hydrophobic microcylindrical arrays by μ-SLA 3D printing", *Journal of Manufacturing Processes*, Vol. 83, pp. 14-26, doi: 10.1016/j.jmapro.2022.08.041.

Wu, C.J., Zhang, T.Y., Guo, W.C., Meng, X., Ding, Z. and Liang, S.Y. (2022b), "Laser-assisted grinding of silicon nitride ceramics: micro-groove preparation and removal mechanism", *Ceramics International*, Vol. 48 No. 21, pp. 32366-32379, doi: 10.1016/j.ceramint.2022.07.180.

Yanar, N., Kallem, P., Son, M., Park, H., Kang, S. and Choi, H. (2020), "A New era of water treatment technologies: 3D printing for membranes", *Journal of Industrial and Engineering Chemistry*, Vol. 91, pp. 1-14, doi: 10.1016/j.jiec.2020.07.043.

Yusoff, H.H.M., Teo, L.I., Phang, S.J., Wong, V.L., Cheah, K.H. and Lim, S.S. (2022), "Recent advances in polymer-based 3D printing for wastewater treatment application: an overview", *Chemical Engineering Journal*, Vol. 429, 132311, doi: 10.1016/j.cej.2021.132311.

Zhan, Y., Yu, S., Amirfazli, A., Siddiqui, A.R. and Li, W. (2021), "Preparations of versatile polytetrafluoroethylene superhydrophobic surfaces using the femtosecond laser technology", *Colloids and Surfaces A Physicochemical and Engineering Aspects*, Vol. 629, 127441, doi: 10.1016/j.colsurfa.2021.127441.

Zhang, H., Sun, W., Wang, L., Wang, J., Wang, S. and Liu, G. (2021a), "A mechanically and chemically stable superhydrophobic coating for preventing marine atmospheric corrosion", *Surfaces and Interfaces*, Vol. 27, 101537, doi: 10.1016/j.surfin.2021.101537.

Zhang, Q., Weng, S., Hamel, C.M.S., Wu, J., Kuang, X., Zhou, K. and Qi, H.J. (2021b), "Design for the reduction of volume shrinkage-induced distortion in digital light processing 3D printing", *Extreme Mechanics Letters*, Vol. 48, 101403, doi: 10.1016/j.eml.2021.101403.

Zhou, W., Wang, J., Zhao, J., *et al.* (2021), "Experimental research on single abrasive grain scratch SiCf/SiC ceramic matrix composite", *Diamond and Abrasives Engineering*, Vol. 41 No. 1, pp. 51-57, doi: 10.3390/diagnostics12010051.

Corresponding author
Chongjun Wu can be contacted at: wcjunm@dhu.edu.cn